From industrial fermentor to CFD-guided downscaling what have we learned?

Haringa, Cees; Mudde, Robert F.; Noorman, Henk J.

DOI
10.1016/j.bej.2018.09.001

Publication date
2018

Document Version
Final published version

Published in
Biochemical Engineering Journal

Biochemical Engineering Journal 140 (2018) 57–71

Contents lists available at ScienceDirect

Biochemical Engineering Journal

journal homepage: www.elsevier.com/locate/bej

Regular article

From industrial fermentor to CFD-guided downscaling: what have we learned?

Cees Haringa[a,b,*], Robert F. Mudde[b], Henk J. Noorman[a,c]

[a] DSM Biotechnology Center, Alexander Fleminglaan 1, 2613 AX Delft, Netherlands
[b] Transport Phenomena, Chemical Engineering Department, Delft University of Technology, Lorentzweg 1, 2628 CJ Delft, Netherlands
[c] Bioprocess Engineering, Biotechnology Department, Delft University of Technology, Lorentzweg 1, 2628 CJ Delft, Netherlands

HIGHLIGHTS

- A comprehensive overview of the Euler–Lagrange bioreactor simulation approach.
- Application of Euler–Lagrange CFD to three different case studies.
- Different strategies to design scale-down experiments using CFD data are discussed.
- Approach selection chart based on hydrodynamic characteristics of modeled reactor.
- The potential of combining Euler–Lagrange CFD with microfluidics is discussed.

ARTICLE INFO

Keywords:
CFD
Euler–Lagrange
Fermentation
Downscaling
Metabolic modeling

ABSTRACT

Euler–Lagrange computational fluid dynamics simulations offer great potential for the integration of transport dynamics and metabolic dynamics in fermentation systems. Since the seminal work of Lapin et al. [1,2], progress has been made, mainly in the analysis of CFD data and translation to laboratory setup designs. Different large-scale processes require different analysis methods; in this paper we discuss which analysis methods are best suited for given reactor types, by reviewing prior simulation cases as well as introducing new test cases. Furthermore, we address challenges in the translation from Euler–Lagrange simulations to laboratory scale systems, and propose methods to work around these shortcomings. Based on the current state of the art, we propose guidelines for the selection of data analysis methods, and we discuss the design of rational scale-down simulators. We conclude with a brief discussion regarding the requirements and possibilities of next-generation scale-down simulators, such as microfluidic single-cell analysis, and possible ways to approximate cellular lifelines from invasive intra-cellular measurements.

Many things are known about scale-up. No longer are Rushton impellers the answer. No longer is our concern only in maintaining the same k_La. Environmental stress due to poor mixing and "hidden" auxotrophy are two factors not fully addressed nor appreciated on scale-up. As a consequence, scale-up is still an art not a science.
Arthur Humphrey: Shake Flask to Fermentor: What Have We Learned? (1998) [3]

1. Introduction

In the past 20 years, "from shake flask to fermentor" (scale-up) has been shifting to scale-down: from industrial-scale to lab-scale. The broth in industrial reactors may be heterogeneous in substrate concentration, dissolved oxygen (DO), shear rate, etcetera. Humphrey, from a scale-up philosophy, hence posed: "we need to learn how to achieve better mixing in large-scale fermentors" [3]. With larger reactors this is increasingly unachievable; heterogeneity manifests due to the competition between mixing and reaction (expressed in the

Abbreviations: CFD, computational fluid dynamics; CRD, computational reaction dynamics; DO, dissolved oxygen; DRW, dynamic random walk; EL, Euler–Lagrange; FACS, fluorescence activated cell sorting; MAMS, micro array mass spectroscopy; PBM, population balance model; (A)PFR, (axially dispersed) plug flow reactor; RTD, residence time distribution; SD, scale-down; STR, stirred tank reactor; UDM, user defined memory; UDF, user defined function

* Corresponding author at: DSM Biotechnology Center, Alexander Fleminglaan 1, 2613 AX Delft, Netherlands.
E-mail address: cees.haringa@dsm.com (C. Haringa).

https://doi.org/10.1016/j.bej.2018.09.001
Received 30 April 2018; Received in revised form 27 August 2018; Accepted 3 September 2018
Available online 08 September 2018
1369-703X/

Nomenclature

A	area (general), m^2
C_s	substrate concentration (mole based), mol/kg
$C_e xt$	generic extracellular concentration, mol/L
$C_i nt$	generic intracellular concentration, mol/g_x
c_s	substrate concentration (mass based), mg/L
C_x	Biomass concentration, g/kg
C_D	drag coefficient, –
D_r	dilution rate, h^{-1}
$\mathcal{D}_m$	diffusion coefficient, m^2/s
$\mathcal{D}_t$	Turbulent diffusion coefficient, m^2/s
F	feed rate (general), kg/s
F_s	Substrate feed rate (general), mol/s
$k_L a$	overall mass transfer coeff., h^{-1}
K_s	affinity constant for substrate, mol/kg
N_s	agitation rate, s^{-1}
N_c	total number grid cells, –
N_p	total number particles, –
$N_{p,c}$	Number particles in cell c, –
q_p	specific production rate of product, $mol_p/Cmol_x/h$
q_s	specific uptake rate of substrate, $mol_s/Cmol_x/s$
$q_{s,max}$	max. specific uptake rate of substrate, $mol_s/Cmol_x/s$
q_{ref}	reference $q_s/q_{s,max}$, –
R_p	reaction rate of s, parcel-based, m
S_s	source term of s, mol/kg/s
S_{ij}	average rate-of-strain (component), s^{-1}
t	time (general), s
U_l	liquid velocity, m/s
U_g	superficial gas velocity, m/s
V	tank volume, m^3
V_c	cell volume, m^3
V_p	parcel associated volume (V_T/N_P), m^3
V_T	total volume (general), m^3
α	gas fraction, –
α_g	geometry constant for no. parcels, –
γ	surface tension, N/m
γ	shear rate, s^{-1}
Δt	timestep size, s
ϵ	turbulent energy dissipation rate, m^3/s^2
θ_{95}	dimensionless mixing time, –
λ	inter-phase mass imbalance (Euler–Lag.), %
μ	specific growth rate, h^{-1}
μ_l	effective Viscosity, dynamic, Pa s
$\mu_{l,eff}$	viscosity, dynamic, Pa s
μ_t	turbulent viscosity, dynamic, Pa s
ρ	density, kg/m^3
τ_{95}	mixing time, s
τ_{arc}	arc-time, s
τ_{circ}	circulation timescale, s
τ_{rxn}	uptake timescale of substrate, s
ϕ_i	circulation flowrate, kg/s
χ	heterogeneity in domain, –
$\Omega_{s,max}$	max. $q_s/q_{s,max}$ on arc trajectory, –

Damköhler number $Da = \tau_{circ}/\tau_{rxn}$), with mixing inherently scale-dependent whereas reactions are microbe-dependent. The scale-down philosophy instead asks how broth heterogeneity will affect process performance, taking the effect of heterogeneity into account early in process development. This approach utilizes "scale-down simulators" (SD-simulators), lab-scale reactors that deliberately produce a heterogeneous environment [4,5]. While developed in the eighties [6–9], SD-simulators gained recent popularity [4] as omics advances enable deeper quantification of the impact of extra-cellular variations on micro-organisms.

A major challenge in downscaling is to devise a lab-scale environment that reflects industrial broth heterogeneity, with only limited knowledge of said heterogeneity. Detailed local substrate/DO measurements are generally lacking for existing processes, and even if flow-following probes enable collection of such data in the future, this is of little help during novel process design. Consequently, SD-simulators are often calibrated without industrial reference [10–12], or based on correlations [6,13]. Such experiments provide valuable insight in the response of micro-organisms to extra-cellular variations, but do not necessarily represent large-scale process performance. Computational Fluid Dynamics (CFD) allows to simulate the hydrodynamics of large-scale reactors, and may provide detailed *in-silico* insight in the microbial environment within fermentors [14,5]. The scale of industrial fermentors prohibits full resolution of turbulence and gas–liquid hydrodynamics, hence approximative models are required [15]. Still, keeping these limitations in mind, CFD offers useful approximation of the large-scale environment, in more detail than offered by correlations or industrial-scale measurements.

CFD is, amongst others, applied to study mixing [16,17], mass transfer [18,19] and substrate gradients [14]. While such studies can supply input for downscaling, the aim of SD-simulators is to capture temporal environmental fluctuations *as observed by micro-organisms*. Euler–Lagrange CFD simulations, in which a large number of virtual particles (parcels) is tracked, are especially suitable: they allow to track extra-cellular environment of each parcel in time (called "lifelines") [1,2]. In our view, these lifelines form a preferential basis for SD-design as they provide detailed dynamic information that is unavailable from purely Eulerian simulations. In a Sino-Dutch collaboration, we explored the use of Euler–Lagrange CFD for SD-design [20]; here we provide an overview of the lessons learned during this project. These lessons include Euler–Lagrange reaction coupling, lifeline analysis methods and their relation to reactor configuration, and scale-down design as well limitations therein. To conclude, we outline some considerations for future scale-down simulators, and present a conceptual design of a micro-fluidic scale-down simulator that may overcome limitations observed for bench scale systems.

2. Bioreactor hydrodynamics

First, the Eulerian model – resolving broth (and air) flow – must be developed. The following aspects are to be considered:

- Macromixing (impeller & gas/liquid interaction)
- Mesomixing (feed mixing)
- Micromixing (e.g. film & intra-pellet mass transfer)
- Aeration (phase interaction, bubble size, etc.)
- Solid-liquid interaction (turbulent motion, settling, etc.)
- Gas–liquid mass transfer ($k_l a$ models)
- Heat transfer
- Rheology (& turbulence/aeration interaction)
- Liquid-microbe transfer/reactions (uptake/excretion)
- Turbulence

The Euler–Lagrange approach is compatible regardless of the choices made regarding the above. Inclusion of all aspects leads to demanding models, while data for modeling and validation may be scarce. Often, one or more aspects are negligible or absent; a timescale/force balance analysis then allows to discard irrelevant processes. Macro-mixing [14], gas–liquid interaction [21,22] and microbial reactions are often considered dominant [14]. Meso-mixing can be relevant near the feed inlet point, where concentrated glucose blobs may be segregated from the broth (hence not observed by biomass) [14,23,24].

Based on the analysis of Linkes et al., eddy micro-mixing and film diffusion are estimated to be rarely limiting [23], although this may differ in highly viscous processes. These aspects may be included via subgrid concentration distribution and film diffusion models, respectively. A concern is that potential mass transfer limitations at the cell surface are rarely checked in experiments, which may compromise the determination of kinetic parameters [25,24]. Even if rarely an issue in practice, it is wise to adopt practices from catalysis engineering to rigorously exclude- or account for them.

Non-Newtonian rheology may be highly relevant [26,27], but is often omitted due to modeling difficulties. In highly turbulent flows, assuming an overall effective Newtonian viscosity $\mu_{l,eff}$ may be allowed, but in transitional flows effective viscosities may differ locally. Moilanen et al. found large stagnant caverns in simulations with a Herschel–Bulkley fluid [27], yielding simulated mixing times in excess of 10 s, compared to ca. 3 s experimentally. While cavern formation may appear in yield-stress fluids, the stagnation observed in these simulations does not appear to reflect reality. They based the local $\mu_{l,eff}$ on the mean flow-shear rate $\gamma = |\partial U_i/\partial x_j|$; it can be argued that the shear rate based on energy dissipation, $\gamma = \sqrt{\epsilon\rho/\mu_{l,\text{eff}}}$, may be more representative. In exploratory simulations we found reasonable single-phase results with this approach, but multiphase simulations diverged (Appendix A). For single cells, the Stokes number $St << 1$ meaning they can be considered massless flow-followers. For cell agglomerates, however, settling effects may become relevant. Turbulent motion of parcels has to be considered. The default way to describe this is via the discrete random walk model (DRW), which may suffer from artificial accumulation of parcels in low-turbulence regions, e.g. near walls [2,28]. Continuous random walk (CRW) models [28] or a Fokker–Planck type treatment [2], may yield superior results. Practically, we observed little accumulation in stirred tanks due to the low surface/bulk gridcell ratio [29]. Possible intra-pellet diffusion limitations can be evaluated via reaction-diffusion models, although determining the intra-particle diffusion coefficient may be challenging. The computational burden makes large eddy simulations unsuitable for (routine) application in bioprocess simulation; cruder Reynolds-Averaged Navier Stokes (RANS) simulations have to be relied on. In reactors lacking significant flow transients (including stirred tanks with the MRF-impeller model), a steady-state solution may be a reasonable approximation, reducing computation time [30]. In the end, the choice of models is dictated by the relevant physics, the required level of detail, and the availability of verification data.

3. Reaction coupling

3.1. Coupling methods

Reactions can be coupled to CFD simulations via regular Eulerian models, population balance models (PBMs), and Euler–Lagrange (EL) models (which are our primary interest). The current focus is on metabolic models [1,2,31,32], and metabolic models including key enzymes [33]. Similar strategies can be applied to include a broader spectrum of cellular responses (transcription and translation dynamics [34–36], protein formation [37], cell cycles [38], and more), provided the resolved timescales are sufficient to capture such dynamics.

Regular and PBM coupling. Regular reaction models compute rates based on the local extra-cellular conditions. This assumes instantaneous equilibrium between intra- and extracellular conditions, which is valid for uptake processes lacking metabolic feedback (for example lacking intra-cellular glucose inhibition) and with constant enzyme capacity, which is justified when considering "process snapshots" of a few mixing times. Directly linking long-term intra-cellular (enzymatic) adaptation to local extra-cellular conditions may lead to gross errors; for example coupling a penicillin production model (enzyme adaptation time $\tau_{ad} \approx 20$ h) to a CFD simulation led to an improbable yield loss of 85% [39]. PBMs account for local non-equilibrium and parcel history by incorporating a transportable distribution of the intra-cellular composition, typically with growth rate μ as a representative parameter. Improved acetate overflow predictions for *E. coli* were found with the approach [31], and and simulations of the full process duration are feasible if (pseudo-) steady hydrodynamics can be assumed [40,41]. Capturing the distribution by traditional class-based methods is tractable for narrow composition ranges (bubble size distributions for example [21]), but becomes cumbersome for broad distributions. Moment methods offer an alternative. Initially, a comparison between 100 and 400 classes and several moment methods found mostly gains in memory use [42], more recently also time-gains were observed [43]. Most studies assume one-dimensional heterogeneity, captured by μ; this may be insufficient in some cases. Consider a model with enzyme X (adaptation time $\tau_X \approx 1\,\text{h} >> \tau_{circ}$) subject to metabolic control by M ($\tau_M \approx 30\,\text{s} \approx \tau_{circ}$). This requires accounting for heterogeneity at two timescales; X may be distributed in the population, but the long turnover time makes the distribution spatially homogeneous. The distribution in M will vary locally, making X and M uncorrelated. Y^n class-interactions may occur for n pools with Y classes, posing a potential computational challenge. Models with two compositional variables have been reported [44]. How the PBM framework performs with higher-dimensional metabolic models is a development to be followed with interest.

Lagrangian coupling. In EL methods N_p individual parcels are tracked. EL simulations come in two forms. EL simulations with Eulerian reaction coupling solely employ the parcels to probe extra-cellular conditions over time, registering what organisms "see" [32,39,22,38]. However, this approach allows for only limited interaction between the extra- and intra-cellular domain [39,33] (see Section 3.2). Reactions can also be coupled to the Lagrangian phase. In this case, the cellular composition is tracked by assigning a composition vector X_n with n pools to each parcel. Each pool is quantified by a single value, making pool interactions straightforward. A metabolic model, taking the extra-cellular concentration field(s) of parcel p as a boundary condition, describes pool and environmental interactions. In contrast to PBM, there are no pseudo-steady states for the Lagrangian phase, requiring a transient solution with short Δt to capture parcel motion and pool dynamics [29]. Typically $O(> 10^5)$ parcels are needed for a smooth biomass distribution [29], making full fermentation simulations infeasible with full Lagrangian coupling. These requirements make EL most suitable to simulate multi-dimensional heterogeneity on minute-hour timescales; the unique parcel perspective provides "lifelines" of the observed environment in time. We do emphasize these models represent an *average* response to extra-cellular variations. At the single-cell level, intrinsic heterogeneity [45] and fluctuations in transcription levels [46] will induce variations in this response, that are not captured by typical metabolic models.

Computational advances are required to enable full fermentation and (faster than) real-time simulations. With innovations in highly parallel and GPU-accelerated CFD giving rise to applications like ANSYS Discovery Live, the prospects are positive, underlining our preference for the EL method. In the next section, practical coupling implementations are discussed.

3.2. Lagrangian coupling: practical aspects

Lagrangian reaction coupling comes with practical challenges, for example regarding N_p. Whether or not full Lagrangian coupling is required depends on how the inter-phase (uptake) reactions are controlled by the cellular composition, where we distinguish three situations:

- C1: no rapid or slow intracellular control.
- C2: only slow intracellular control.
- C3: only rapid or rapid and slow control.

The cases are graphically summarized in Fig. 1. In C1, uptake reactions are completely uncoupled from the Lagrangian phase, meaning straightforward Eulerian reaction coupling can be employed and parcels are only used to register extra-cellular fluctuations [32,39,22,38]. The number of parcels N_p needs to be sufficient to converge fluctuations statistics (typically 10^0–10^4, depending on resolved flow-time), but is otherwise unrestricted. The assumption of no intra-cellular control (e.g. simple Monod kinetics with constant parameters) is valid if there are no rapid turnover intra-cellular pools ($\tau_{pool} < \tau_{mix}$) controlling the rate (or: instantaneous equilibrium can be assumed), while changes in slow pools ($\tau_{pool} \gg \tau_{mix}$) are insignificant (growth and enzyme dynamics can be neglected in the chosen timeframe). Intra-cellular responses can be calculated in the CFD software or during post-processing, as there is no feedback to the Eulerian phase.

In C2, growth and/or enzyme level changes have to be accounted for, and the population may exhibit significant heterogeneity in enzyme levels. However, since $\tau_{pool} \gg \tau_{mix}$, the population distribution will be the same everywhere in the domain. This allows a hybrid Euler–Lagrange model: uptake reactions are coupled to the Eulerian phase, but reaction parameters like $q_{s,max}$ are determined based on on population average enzyme levels [33] in the Lagrangian phase. In this case N_p must suffice to capture enzyme pool distributions. In C3, local uptake/excretion rates are affected by intra-cellular heterogeneity in rapid turnover pools, which requires full Lagrangian coupling to capture [1,2]. In this case, the distribution of parcels determines the distribution of biomass, and N_p must be sufficient to produce a (near) homogeneous biomass distribution, in order to ensure realistic concentration fields. This puts a criterion on N_p [29] that is treated in the next section.

```
Timestep t
{
Update Eulerian Fields (U,V,W,Cext)
(implicit loop over cells c)
transfer user-defined memory to cell source terms
Ss(c) = UDM(c)
Cext(c,t)= Cext(c,t-1) +  Ss(c)*dt                [mol/L]
Reset source terms
UDM(c)  = 0
}

Loop over P particles
{
Determine cell c containing particle p,
determine reaction rates
Rp(p,t) = f(Cext(c,t),Cint(p,t-1))                [mol/gx/s]
Update intra-cellular pools
dCint(p,t-1)/dt = Rp(p,t)                         [mol/gx/s]
Cint(p,t) = Cint(p,t-1) + dCint(p,t-1)/dt *dt     [mol/gx]

Update extra-cellular sources
Store in user defined memory(c)
UDM(c) = UDM(c) - Rp(p,t)*Cx(p,t)         [mol/L/s]

Store extra- and intra-cellular values in file
}
transfer to next timestep
```

Fig. 2. Pseudocode for an (explicit) implementation of parcel-bound kinetics in ANSYS FLUENT. Updating the reaction-rates and intracellular pools is done using a *DPM scalar UDF*. Uptake rates are transferred to used defined memory (UDM) and included in Eulerian computations in the next timestep via source term UDFs. An *execute at end UDF* is used for data storage, and to reset the UDM.

3.2.1. C3: interphase coupling

In Lagrangian coupling, inter-phase species transfer is key; uptake by parcels must equal field depletion. The pseudocode in Fig. 2 describes an (explicit) implementation of parcel-bound kinetics in ANSYS FLUENT. The workflow in FLUENT means DPM scalars, and hence source terms S_s, are updated *after* the field iterations: what parcels consume in step t, is taken from the extra-cellular domain in step $t+1$. Aside from challenges with explicit integration, an issue is that the mass balance is violated if uptake exceeds availability ($S_s(c,\ t)\Delta t > V_c(c)C_s(c)$) [29]; source term 'clipping' will occur. As parcels do not "see" each other, this may also occur when multiple parcels reside in the same gridcell, competing for the same substrate. Re-calculating the exchange terms in each iteration accounts for the presence of multiple parcels (uptake now fully takes place in timestep t), but increases computational expense, and it was not found to yield improved accuracy [29]. In fact computing q_s once per timestep performed slightly better, possibly due to exploiting sub-flowtime time-stepping for parcel updating. In open-source or dedicated codes, an implementation that combines sub-flowtime stepping with implicit integration may be more

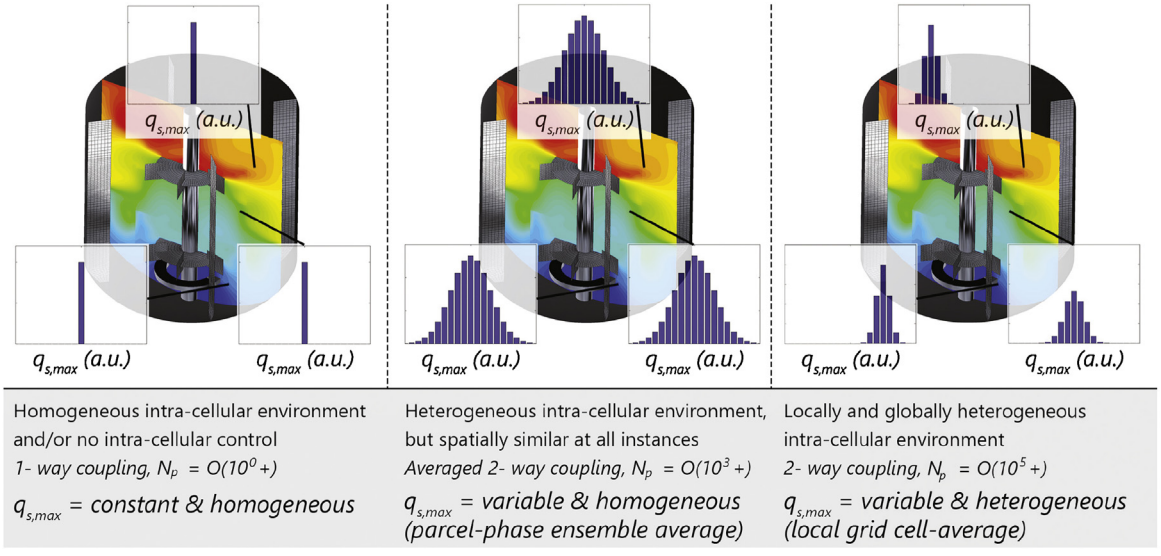

Fig. 1. Coupling approaches used in this work. *Left:* C1: instantaneous intra-cellular response or constant intra-cellular environment, leading to a homogeneous population. *Middle:* C2: slow intra-cellular variations, leading to a heterogeneous population, but without spatial variation. *Right:* C3: rapid intra-cellular variations, leading to a population distribution that is also spatially heterogeneous. The shown distributions are hypothetical distributions on the single-cell level. In practice, the resolved number of parcels in current Euler–Lagrange simulations does not suffice to *locally* reconstruct such instantaneous distributions of cellular composition.

straightforward to implement than in commercial codes.

3.2.2. C3: simulation criteria

To resolve flow dynamics for many parcels requires a proper balance between computational burden and accuracy; N_p and timestep Δt have a large influence. It is clear from the pseudocode that if $N_p << N_c$, $S_s = 0$ in many gridcells, i.e. no biomass will be present, resulting in unphysical q_s and C_s gradients. The volume of gridcells in a locally refined grid may range over orders of magnitude, meaning some cells contain many parcels, while others are mostly empty even if $N_p \gg N_c$; ensuring homogeneity by increasing N_P is unrealistic. An alternative, distributing q_s in a parcels 'effective volume' $V_p = V_{domain}/N_p$ requires cumbersome listing of surrounding gridcells. However, if turbulent distribution of substrate is sufficiently fast, artificial gradients will be minor even with inhomogeneous parcel distributions. By linking the magnitude of unphysical gradients to the ratio of timescales of reaction and turbulent dispersion, and including fluctuations in parcels-per-cell $N_{p,c}$, a criterion for N_p can be developed. Substituting the timescales with the underlying hydrodynamic and kinetic parameters this gives (for Monod and 1st order kinetics) [29]:

$$N_p = \alpha_g^2 \left[\frac{q_{s,\max} C_x}{K_s \chi \sqrt{V_T}} \sum^{N_c} \left(\frac{V_c^{7/6}}{\mathcal{D}_{t,c}} \left(1 - \left(\frac{V_c}{V_T} \right) \right)^{1/2} \right) \right]^2 \quad (1)$$

With χ an accuracy parameter and α a geometry-dependent constant. For typical conditions, this gives $N_p = 10^4$–10^6 if $\chi = 0.05$. With this, running full fermentation simulations ($O(> 10\,\text{h})$ on desktop computers is infeasible, but several mixing times (O(min–h)) to gain insight in metabolic fluctuations are manageable. A timestep size of min $(1/(10N_s), \tau_{rxn}/10)$ is advised for stirred tanks, with N_s the stirring speed in s^{-1} and τ_{rxn} the timescale of the fastest exchange reaction [29]. The first of these criteria considers flow trajectory calculation and may differ per reactor type. The pioneering studies by Lapin et al. did not explicitly note the effect of parcel distribution on uptake; with 10^5 parcels in 44^3 gridcells [1,2], their work was likely in accordance with these criteria. All criteria are based on 1st order accurate explicit integration for the exchange terms; the presence of stiff intracellular reactions may change the criteria and favor the use of higher order explicit or implicit methods, at least for the intra-cellular equations.

3.2.3. Model structure

Dynamic kinetic models should be designed with CFD in mind, meaning they should be stable towards turbulent fluctuations in extracellular concentrations C_s. Using a model for penicillin production [47], two potential issues were identified: (1) noisy rates when extra-cellular control was assumed over intra-cellular rates and (2) non-zero rates at zero pool size [33]. Concerning the first, storage of glycolitic intermediates to polymers was non-linearly controlled using extra-cellular substrate as a signal molecule, strongly affecting rates in the range of turbulent fluctuations. Rates hence oscillated rapidly, inducing insufficient release of storage carbohydrates during starvation, which reduced ATP availability. Such issues (and numerical issues noted above) are more likely present in systems with low K_s, as small C_s variations may lead to strong q_s variations. Low X_{ATP} quenches depolymerization, while the ATP-consuming storage process continued (a non-zero storage rate at low X_{ATP} was no realistic scenario in model development), eventually driving X_{ATP} negative.

Numerical instability was excluded as a cause by varying integrators (implicit, explicit, RK4), timestep sizes ($\Delta t = 0.0005$–0.5 s), and enforcing noise in MATLAB. The issues related to the non-linear differential-algebraic formulation of the model, not to the solution algorithm. The problem was bypassed by correlating X_{ATP} with the glycolitic pool X_{GLY}, but storage rate oscillations remained [33]. More generally, direct extra-cellular rate control over intra-cellular rates should be avoided (instead, use intra-cellular substrate, ATP or redox factors as a signal), or a signaling timescale should otherwise be introduced, for example using an "activated enzyme pool", to buffer rapid extra-cellular dynamics. Furthermore, ensure all rates quench when their reactants deplete, even if depletion is unlikely. Most dynamic metabolic models described in literature are based on ideal-mixed systems with smooth dynamics, not anticipating CFD application. For example, Lei et al. [48] eliminated all intra-cellular pools for *S. cerevisae*, as intra-cellular changes could be considered instantaneous compared to slow (fed-) batch dynamics. Imposing rapid noise on this model led to similar issues as described above. We did not conduct rigorous stability analysis, which may be a future avenue to formalize model requirements.

3.2.4. Compartment-based Lagrangian simulations

The high N_p required to simulate the microbial phase induces a large computational burden. With C3 coupling and unsteady hydrodynamics,

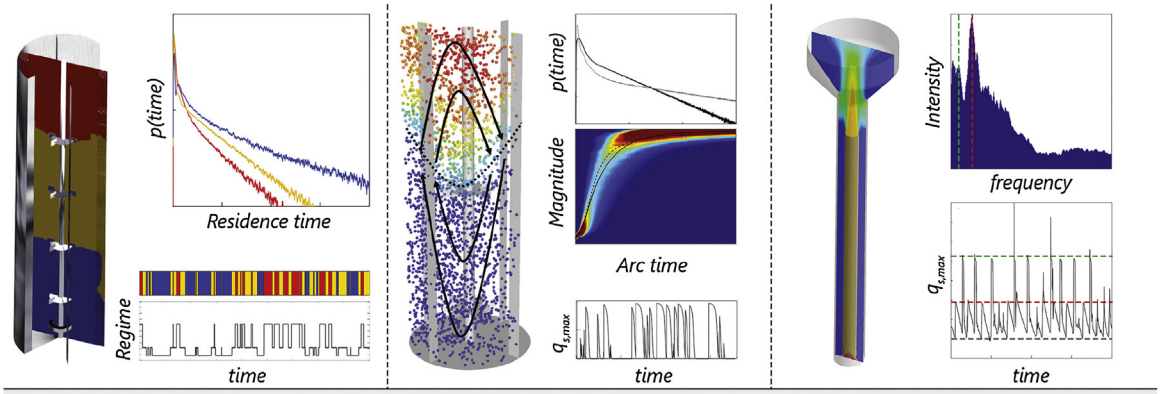

Fig. 3. Lagrangian analysis methods used in this work. *Left:* Regime analysis, based on regions in q_s-space with a consistent metabolic response. Most suitable for compartmentalized flows (often found in stirred tanks), and for application with multi-compartment downscaling. *Middle:* Arc-analysis, based on the duration between subsequent crossings of a reference value in q_{ref}. Most suitable for non-compartmentalized flows (smooth extra-cellular variations), with a wide residence time distribution (some stirred tanks, bubble columns) (*Right:* Fourier analysis, seeking the dominant fluctuation frequencies. Most suitable for flows with narrow residence time distributions, such as airlift-loop or pipe reactors. Here, methods were illustrated with q_s variations, but they are broadly applicable.

simulating several mixing times can take weeks on a desktop computer; in contrast, a full fermentation period is feasible in 1–2 weeks assuming steady state flow and C1–C2 reaction coupling. Using the hydrodynamics of compartment models using CFD, and modeling (Lagrangian) reactions in these compartment models, can strongly reduce computation time by lowering both N_p and grid size N_c, without severely compromising accuracy [49,50]; parcel tracking in such a model can be done, for example, using a statistical (Markov-chain) rather than a trajectory-resolved approach [51–54].

4. Lifeline analysis methods

Lifelines represent cellular data as a function of time, and can be subjected to signal/statistical analysis to report extra-cellular fluctuations experienced by organisms. One of the main goals of lifeline analysis is to provide guidance in the design of scale-down experiments. The methods described below aim to capture statistics describing the duration and magnitude of extra-cellular fluctuations, which can then be used to set design parameters for scale-down simulators (as described in Section 5). To our knowledge, such a direct CFD-based scale-down design has not yet been used, at least in public literature. There are, however, examples where scale-down design was aided by CFD results, for example in setting the order of magnitude in fluctuation frequency, shear-rate or fluctuation amplitude [55–58].

Three methods were addressed: Fourier analysis, Arc-analysis and Regime-analysis. A graphical overview of methods is provided in Fig. 3. The preferred method depends on:

- Flow behavior (plug-like or well circulating).
- Compartment formation.
- Operating conditions.
- Application (downscaling method).

Low-pass filtering of lifelines to remove rapid turbulent variations is advised, as these are unlikely to have metabolic influence and may affect the statistics of large scale fluctuations. Smoothing using the timescale of turbulent fluctuations as a window is the most straightforward approach [39].

Fourier analysis. The Fourier method is fast and straightforward, giving most insight with periodic fluctuations, e.g. narrow circulation time distributions. For broad distributions, data interpretation is challenging [39]. First, the mean is subtracted from the lifeline (as a reference value) which is then multiplied with a window function and fed to an FFT algorithm. The real parts of the transforms are subsequently

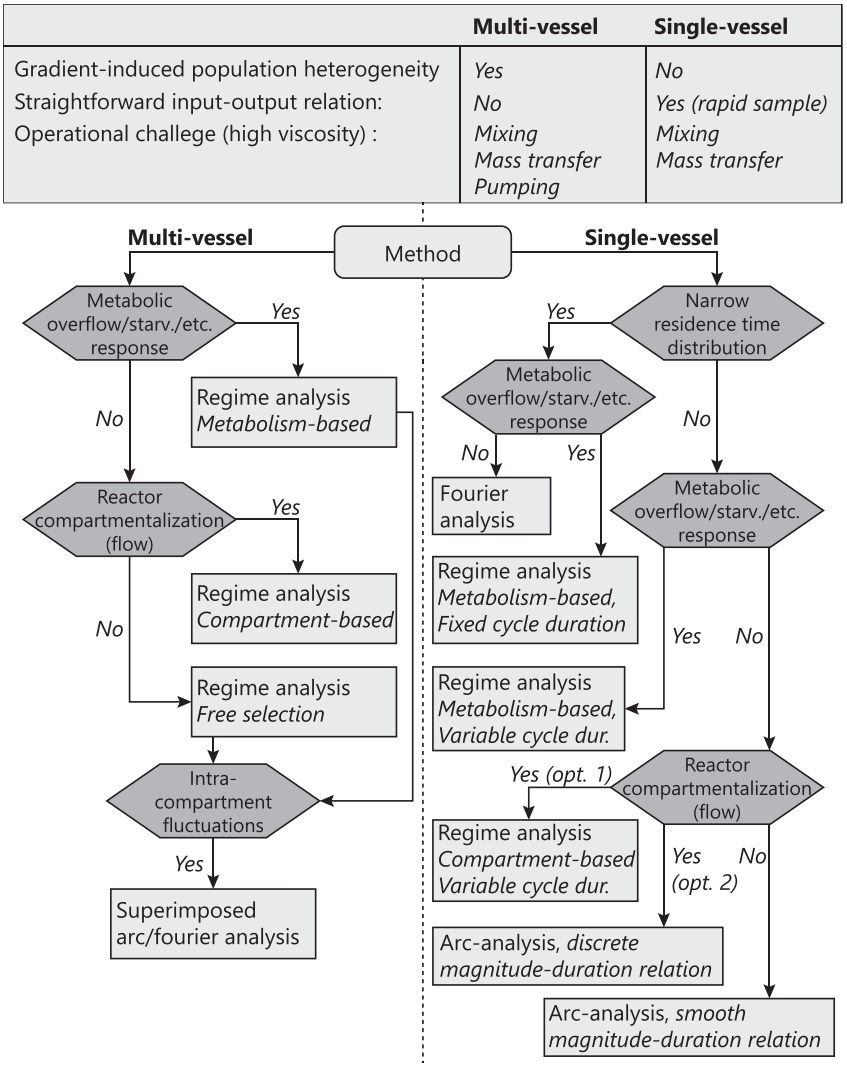

Fig. 4. Analysis selection diagram. Top: some considerations for SD-selection. Gradient-induced population heterogeneity means different cells have significantly different lifelines (In single-vessel scale-down simulators, some difference between individual cell experiences may exist by micro-mixing, but all cells experience the same *explicitly induced* variations). Operational challenges are linked to pumping issues for shear-sensitive and complex rheology systems. The selection chart gives the *preferred* analysis method; other analysis methods may still be applicable.

summed to a composite spectrum to reveal dominant frequencies. Amplitudes are retrieved by visual inspection of the lifelines; extracting them from spectra is more challenging.

Arc-analysis. Arc-analysis records fluctuations compared to a reference q_{ref} (e.g. the mean) in the time-domain [39,22,33]. The interval between consecutive q_{ref} crossings gives the fluctuation duration, akin to a circulation time measurement in reactant rather than physical space. The magnitude follows from the extreme lifeline value between crossings; correlating magnitude and duration provides insight in typical circulation trajectories. The three points (start, extreme and end) form an "arc" describing the fluctuation. The time at which the maximum is recorded can be used to study if fluctuation trajectories are symmetric. To remove negligible oscillations, it is advised to only register events that exceeding q_{ref} by a certain threshold. A drawback arc-analysis is that secondary motions are not captured; the method is most applicable for relatively simple circulation behavior, not for strongly compartmentalized reactors.

Regime analysis. In regime analysis, the domain is divided into zones based on a characteristic quantity such as a certain metabolic response (e.g. $C_s > C_{s,overflow}$), or a relatively homogeneous concentration (a compartment around an impeller) [39,22]. The fluctuation duration follows from the duration of individual regime visits. Again, it's advised to set a crossing threshold (a "fuzzy boundary" [29]) to remove minor fluctuations. The amplitude is replaced by a per-regime mean value; if oscillations around this mean are relevant, arc-analysis can be conducted *within* a regime. Regime analysis works well with more complex systems, like compartment-forming multi-impeller reactors.

The role of downscaling. Fourier and arc-analysis are best suited for single-vessel, fluctuating input designs. Both provide the duration (distribution) of observed fluctuations, and the amplitude compared to a reference value. Regime analysis directly links to multi-vessel scale-down, each vessel representing a regime, operating at the regime mean. This means that the number of regimes may be practically constrained [22]. For a combination of feed fluctuations and multiple vessels the combination of regime and arc-analysis seems most applicable. The preferred downscaling method follows from lifeline structure (smooth versus discrete jumps) and practical considerations. In a single vessel SD-simulator, all organisms see the same; the effect of rare, extreme fluctuations cannot be captured. A multi-vessel simulator accounts for the duration distribution by design, but it does not account for the

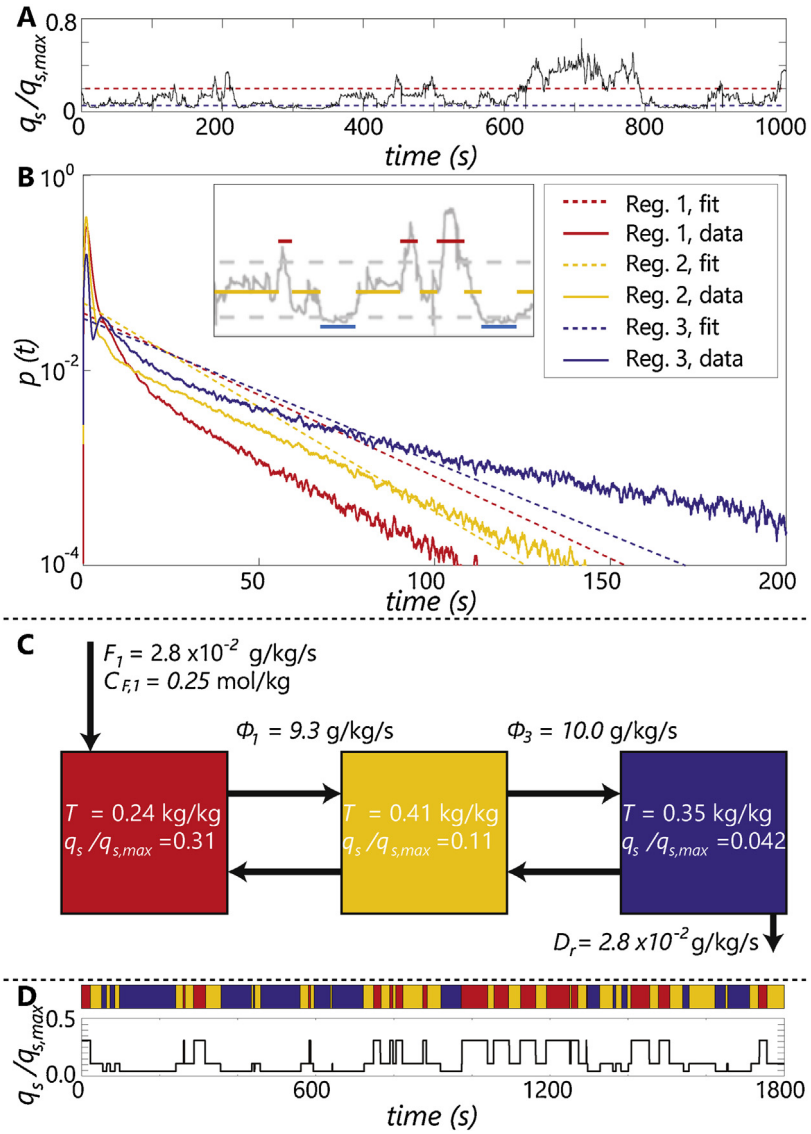

Fig. 5. Analysis of Case I. *A:* Example lifeline, the red and blue dashed line providing regime boundaries. *B:* Residence time distributions (RTDs) per regime (solid lines), fitted ideal stirred tanks RTDs in a 3-vessel SD-simulator (dashed). The volumetric regime distribution is reported in Fig. 3A; the inset shows conceptual lifeline discretization. *C:* 3-vessel SD-simulator based on the regime division, RTDs, and regime-mean operating conditions. *D:* Example of a SD-simulator lifeline. Image reproduced from [22] with permission.

Table 1
Validation of airlift loop simulations, compared with experimental data of Simcik et al. [65].

Parameter	Simulation	Experimental
u_l (m/s) (draft tube)	0.7	0.75
u_l (m/s) (downcomer)	0.18	0.18
α (draft tube)	0.06	0.07
α (downcomer)	0	0.02

amplitude distribution; this is better captured in fluctuating input systems. Single-vessels are also more straightforward to operate and analyze. Sweere et al. [7–9] and Wang et al. [55] are among the few to compare two downscaling approaches. Both observed significantly different responses at equal mean fluctuation time, including hints at different substrate transporter expression, showing that an increased understanding of the metabolic response to extra-cellular variations is still required. In Fig. 4 we present a selection chart for the preferred analysis method depending on the problem statement and downscaling approach, built on our experience to date.

5. Case studies

Three different case-studies were explored in this project, with different lifeline structures and analysis methods.

5.1. Case I: stirred yeast fermentation

A top-fed stirred, aerated yeast fermentation in a 22 m^3 research fermentor was simulated [14,59–61,56]. Details regarding computation and validation are found in [22]. The analysis considers a short time-frame (ca. 1800 s). Monod kinetics for glucose consumption were assumed, using C1-coupling; dissolved oxygen and ethanol were not simulated. The observed concentration gradient is in decent agreement with experimental data [14]. Eight circulation loops form around the 4 impellers, yielding strongly compartmentalized flow; regime-analysis is the preferred analysis method. The reactor circulation time $\tau_{circ} \approx 40$ s is close to the characteristic reaction time $K_s/C_x q_{s,max} = 38$ s which suggests a global gradient. The per-loop circulation time is $\tau_{loop} \approx 40/8 \approx 5$ s, making the individual compartments well mixed.

7 q_s ranges can be discerned [22]. While a 7-regime analysis can be conducted, the q_s jump between compartments is small, and the average residence time impractically short. A 3-regime division is therefore selected, in line with state of the art downscaling [62]. The boundary between regime 1 and 2 is set to $q_s/q_{s,max} = 0.05$ to capture the large, nearly homogeneous bottom region. The regime 2–3 boundary is set to $q_s/q_{s,max} = 0.2$, the expected transition to Crabtree ethanol fermentation [63]. The regime layout is provided in Fig. 3A, the lifelines in Fig. 5A. From the acquired regime residence time distributions (RTDs) (Fig. 5B), it is possible to design a multi-vessel SD-simulator using the 5 degrees of freedom posed by Noorman [64]:

- Number of regimes → number of reactors.
- Per-regime volume fraction → Reactor volume ratio.
- RTD → Reactor circulation pattern.
- Mean RTD, regime volume → Exchange flowrates.
- Mean regime conditions → Feed/aeration rates.

Despite the complex flow patterns, each regime RTD shows the exponential decay of a recirculating flow (Fig. 5B); 3 well-mixed compartments are hence selected. The exchange flowrates are found by fitting the regime RTDs with perfect stirred-vessel RTDs (Ignoring the short term peaks, and under the restriction that $\Sigma(\phi_{circ}) = 0$). Knowing the flowrates, MATLAB optimization is used to specify feed and drain rates, leading to the design in Fig. 5C, with an example lifeline depicted in Fig. 5D. In order to set the operating q_s, the SD-system needs to operate at or above $C_x = 15$ g/kg; the underlying reason is further discussed in [39,22].

5.1.1. Case study II: airlift yeast fermentation

The forced flow structure in an airlift loop reactor leads to a more narrow RTD [66,67], which is revealed in the lifelines. Lacking an industrial case, we simulated a hypothetical fermentation based on the geometry and conditions of Simcik et al. [65]. A bubble size of 5 mm was assumed. The realizable $k-\epsilon$ turbulence model, Universal drag model and Simonin et al. turbulent dispersion model were used [68]. 2nd upwind discretization was used except for volume fraction, for which 1st order upwind was used to ensure stability. Validation results are in Table 1. We employed the yeast kinetics used in case I with a biomass concentration of 30 g_{dw}/kg. The liquid phase properties equaled water, for air $\rho = 1.2$ g/L, $\mu_l = 18.6 \times 10^{-6}$ Pa s were set. Profiles of steady-state holdup and liquid velocity are shown in Fig. 6A, B.

The feed $F_s = 0.00194$ mol/s, included as a source term at the bottom of the draft tube, at the high-q_s spot in Fig. 6C. The feed was set such that under ideal mixing conditions $K_s = C_s$. The non-ideal simulated conditions result in a gradient ranging from $0.45 < q_s/q_{s,max} < 0.8$. 7500 particles were tracked for 200 s. Fig. 7 shows a typical track, showing periodicity, in contrast to those from stirred vessels. Still there is duration variability, from two sources: 1) dispersion in the riser/down-comer and 2) recirculation in the headspace. Two 'types' of peaks are distinguished in the lifelines; peaks with $q_s/$

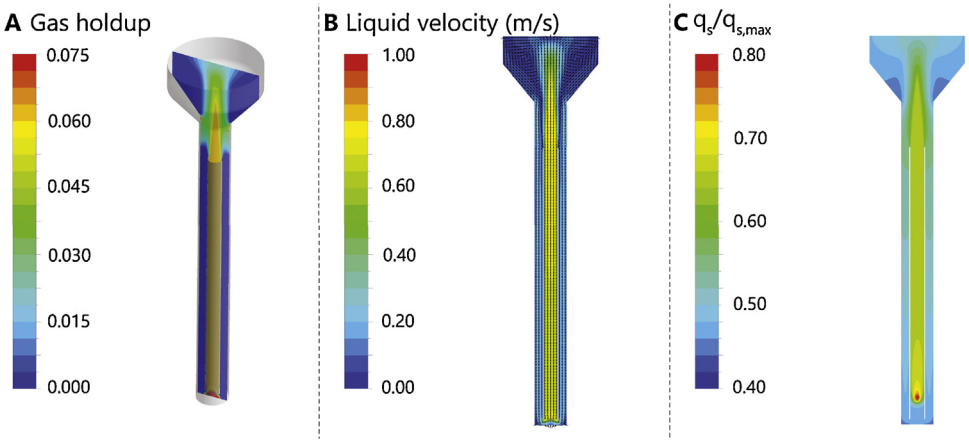

Fig. 6. Eulerian profiles for the Airlift loop reactor. *A:* Gas holdup profile. *B:* Liquid velocity profile. Vectors show direction, colors show magnitude. *C:* Uptake rate profile. Substrate is fed right above the sparger, leading to a high-uptake hotspot at this location.

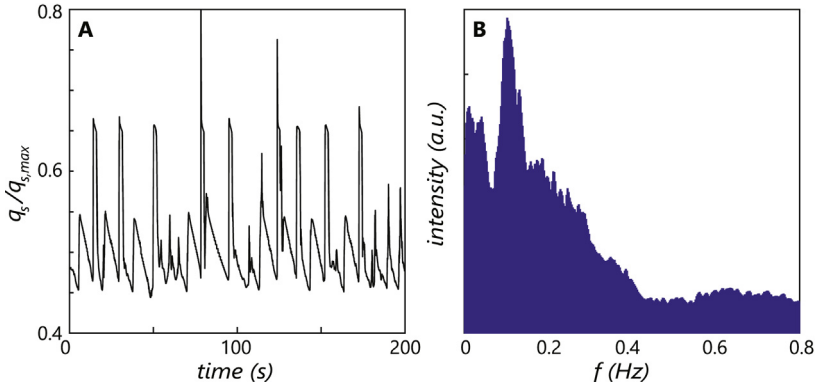

Fig. 7. *A:* Single lifeline in the airlift-loop reactor. *B:* Composite Fourier spectrum of 7500 tracks, peaking at 0.05 and 0.11 Hz, associated with reactor and headspace circulations respectively.

$q_{s,max} > 0.6$ from feed point passages, peaks with $0.52 < q_s/q_{s,max} < 0.6$ from down-comer passes and headspace recirculation; a high peak followed by a low peak is a direct full circulation, a high followed by multiple lows signifies repeated headspace recirculation. The riser peaks are uniform, reflecting the uniform velocity profile; the recirculation/downcomer peaks show more variability. The periodic nature makes the lifelines more suitable for Fourier analysis than prior examples. The combined spectrum of 7500 lifelines (Fig. 7) shows two distributed peaks centered around 0.05 Hz and 0.1–0.12 Hz, the first reflecting the interval between feed-passings, the second reflecting the secondary circulations.

Three straightforward scale-down strategies can be devised: (1) a variable feed reactor, total cycle time of 20 s (0.05 Hz), imposing $q_s/q_{s,max} \approx 0.65$ at the cycle start, optionally using a secondary injection at $t = 10$ s to reach $q_s/q_{s,max} \approx 0.54$. (2) A STR-PFR combination with the STR representing the headspace/downcomer and the PFR as the riser, containing the feed point (Fig. 8A). (3) A 2-PFR combination, one near-perfect PFR for the riser and a more dispersed PFR for the headspace/downcomer (Fig. 8B). Putting the "riser" above the "downcomer" compartment has the benefit of allowing selective aeration in the "riser" section, if combined glucose and oxygen gradients are desired. We present conceptual designs for systems (2) and (3), by fitting the $q_s/q_{s,max}$ distribution between the CFD results and idealized systems using the MATLAB function *fmincon*, assuming the system in chemostat operation with a dilution rate $D_r = 0.05\ h^{-1}$ and $C_x = 30$ g/kg. The fitted parameter values are reported in Fig. 8A, B, for concept 2 and 3,

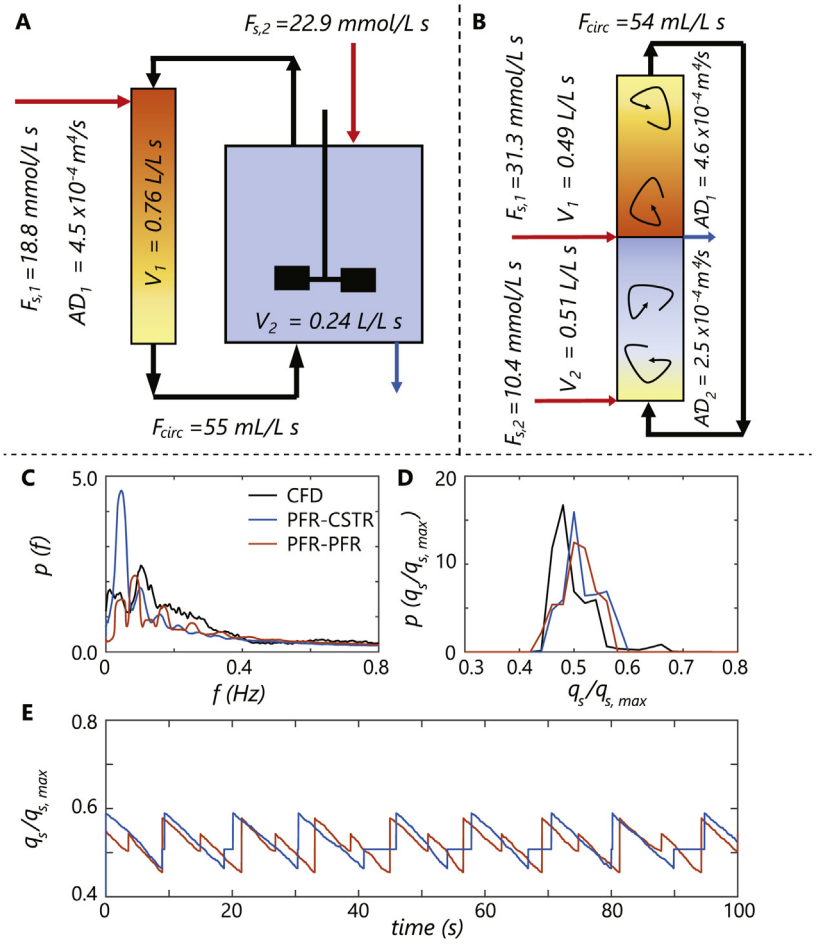

Fig. 8. Conceptual design of multi-vessel SD-simulators for the airlift case. *A, B:* Sketches of the PFT-CSTR and PFR-PFR configuration, respectively, with design parameters as determined by fitting the $q_s/q_{s,max}$ distributions. Note the desired axial dispersion depends on the reactor cross-sectional area *A C:* Frequency spectra for the lifelines in both designs, compared with the CFD result. *D:* $q_s/q_{s,max}$ distribution for both designs, compared with the CFD result. *E:* Examples of lifelines for the scale down simulator designs proposed in *A, B*, generated using idealized CSTR/axially-dispersed PFR models in MATLAB. These lifelines are designed to replicate the airlift-loop lifelines reported in Fig. 7A.

respectively. Fig. 8C–E shows the Fourier spectrum, $q_s/q_{s,max}$ distribution and example lifelines, respectively. Note the Fourier spectrum was not fitted – by requiring a similar $q_s/q_{s,max}$ distribution a decent frequency spectrum match emerged automatically. Due to rapid dilution near the feed point in CFD simulations, the peak in $q_s/q_{s,max}$ cannot be reproduced explicitly.

5.1.2. Case study III: stirred penicillin fermentation

A broad study with both C1- and C2-coupling was conducted in a 54 m^3 stirred fermentor (described in [39,33]), using the metabolic model by Tang et al. [47] with adaptations to ensure stability [33]. The effect of viscosity was omitted due to divergence. The mixing time overestimated experimental data by about 25% with aeration included, excluding aeration gave a similar under-estimation. With $\tau_{rxn} = 0.32$ s and $\tau_{circ} \approx 26$ s, a strong gradient appeared, which manifests itself completely in the top impeller loop, with the vessel bottom operating under starvation conditions. For end-of-fermentation snapshot simulations ($C_x = 55$ g/L, C1-coupling), a penicillin yield Y_{sp} loss up to 40% is found, depending on the circulation time. A linear relation between Y_{sp} and Damköler number τ_{circ}/τ_{rxn} is observed in the range, allowing for interpolation. The single-loop gradient gives smooth fluctuations with a wide duration distribution (Fig. 9A), suitable for arc-analysis (Fig. 9B,C).

Setting $q_s/q_{s,max} = 0.05$ as q_{ref}, only arcs above q_{ref} have to be analyzed in magnitude, showing a clear relation between duration and magnitude (Fig. 9D,E). Below q_{ref} assuming $q_s \rightarrow 0$ and registering duration suffices. From this data, an SD-simulator with variable intervals can be designed. Using inverse transform sampling, a string of random intervals can be generated that abides the duration pdfs (Fig. 9D), alternating between positive and negative (Fig. 9F,G). For positive arcs, the amplitude is set from the duration-magnitude relation, computing the feed from the mass balance. In-silico assessment of the SD-system assuming ideal mixing shows good agreement in yield loss compared to large scale CFD.

In-silico assessment allows to study simplifications; faithfully reproducing the arc structure (Fig. 9F), with gradual feeding followed by consumption, requires the industrial $C_x = 55$ g/kg. This may be challenging to operate with filamentous fungi at SD scales. It is found that administering the pulse instantaneously and reducing the consumption rate by halving C_x (Fig. 9G) does not affect the predicted cellular response, while theoretically reducing the viscosity by a factor 5.6 [26]. Furthermore, with finite mixing times of 2.2 and 13.2 s the predicted metabolic response still equals ideal mixing, implying the SD-protocol is realizable in practice. If lower C_x and/or regularly spaced pulse intervals are required, faithful downscaling based on extra-cellular variations is not possible for the simulated conditions. An alternative is to conduct "intra-cellular downscaling": finding a set of inputs that replicates the metabolic model output (q_p, μ and/or intra-cellular pool

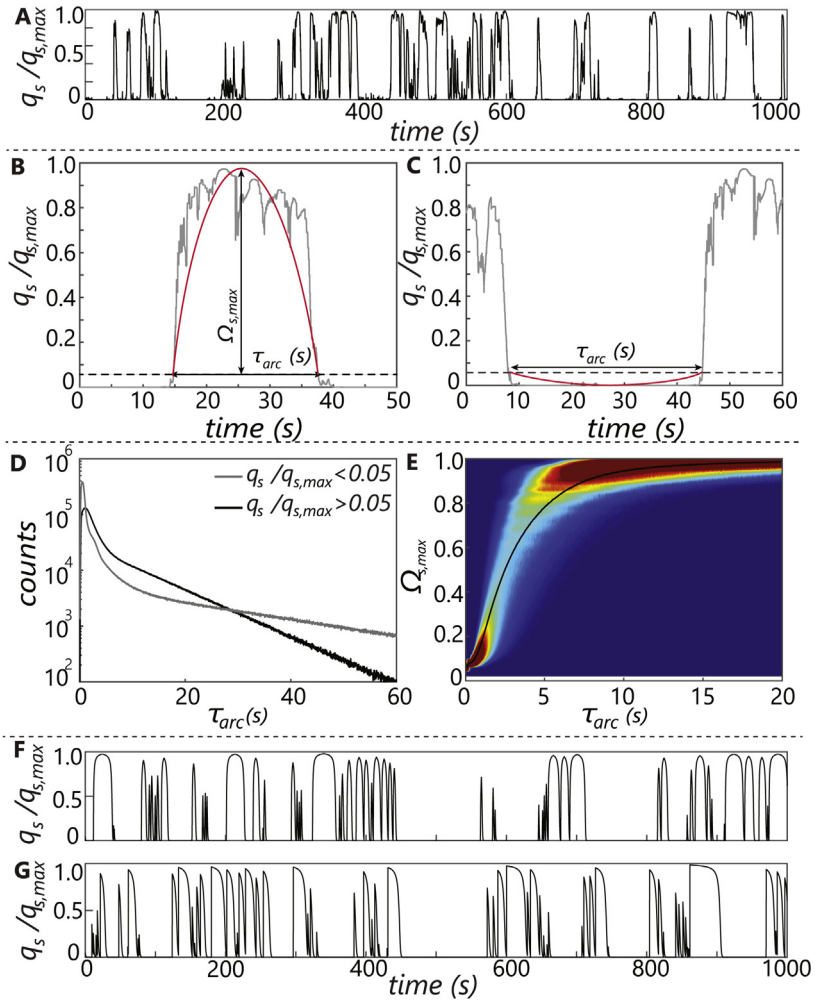

Fig. 9. *A:* Lifeline for case III. *B, C:* Arc analysis approach with $q_{ref} = 0.05q_{s,max}$. *D:* Arc time distributions based on all lifelines. *E:* Relation between arc-duration and magnitude. The solid line gives the mean magnitude as function of duration. *F:* SD-lifeline generated from the arc-time distributions and magnitude. Feeding is gradual, with $C_x = 55$ g/kg. *G:* Alternative feed protocol with instantaneous pulses allows to set $C_x = 27.5$ g/kg. A comparison with the metabolic model of Tang et al. [47] showed no significant difference in metabolic response [33]. Image reproduced from [33] with permission.

sizes) within set constraints (fixed feed period, pre-set C_x). This can be done by feeding intra-cellular target values and constraints to a genetic algorithm for optimization [69], for brevity a further discussion is in Appendix B.

Besides downscaling, CFD-CRD (Computational Reaction Dynamics) for design optimization and full fed-batch simulations are explored. Moving the feed from the top to the impeller discharge stream reduces the projected yield loss from 31% to 9%. To conclude, fed-batch simulations with C2-coupling were conducted; the predicted yield-drop agrees with experimental observations. The model predicts significant heterogeneity in the number of glucose transporters depending on the cellular history. This observation has not yet been experimentally assessed, but it shows the capacity of simulations to generate hypothesis for experimental follow-up. All-together, this case highlights the spectrum of applications of coupled CFD-CRD [33].

5.2. Other Euler–Lagrange studies

The major aspect not addressed in the Sino-Dutch collaboration is C3-coupling with metabolic models; guidelines for C3-coupling were explored with a Monod-model, while the *P. chrysogenum model* lacked rapid feedback and did not warrant the computationally expensive approach. The seminal work of Lapin et al. remains the sole example of C3-coupling, exemplified by replicating experimentally observed NADH oscillations in a yeast culture [1] and gradients in the phosphoenolpyruvate to pyruvate ratio in *E. coli* [2]. C1-tracking has been used more frequently; McClure et al. quantified the duration of substrate fluctuations in a bubble column [32]. Kuschel et al. simulated an *E. coli* cultivation and used regime analysis for transitions between replication regimes; they linked the transition frequency to experimentally transcriptome changes [38]. Liu et al. [70] used Euler–Lagrange simulations to study shear exposure of plant cells, linking the death rate to peak shear exposures in a lifeline extension of the EDCF function [71]. Delafosse et al. used a CFD-based compartment model, to compare trajectories with experimentally recorded tracks [54].

6. Towards novel scale down simulators

Current generation downscaling approaches have inherent limitations: all cells observe the same in single-vessel systems, and both in single and multi-compartment systems, a limited range of frequencies/amplitudes is available, with no straightforward way to reduce glucose concentration other than by consumption alone [39,22] (for oxygen, there is the option of stripping with an inert gas). While current scale-down simulators operating at industrial C_x may capture dynamics at the average level, more rapid dynamics at the individual level are unattainable. Formulating the desires for a new generation of SD-simulators:

- Decouple rate-of-change from consumption.
- Full range of amplitudes can be imposed.
- Full range of durations can be imposed.
- Arbitrary duration (circulation) patterns.
- Different cells undergo different experiences.

It would additionally be desirable if individual or small sub-populations of cells could be analyzed, to gain insight in individual experiences rather than population averages. It may be challenging to satisfy all the above, but there are promising developments in microfluidic development [69]

6.1. Towards microfluidic downscaling

Microfluidic devices allow to conduct small-population or even single-cell cultivation. They have been applied to study growth under controlled conditions [72–76], and to study enzyme dynamics during slow extra-cellular variations [77,78], but not to impose rapid fluctuations (to our knowledge). Convective flow can renew volumes in less than a second in typical micro-cultivations, and with a diffusion coefficient $\mathcal{D}_m = 6 \times 10^{-10}\,\mathrm{m^2/s}$ (glucose in water), diffusive transport over a typical 50 µm lengthscale takes around a second. Theoretically, all but the most rapid turbulent variations can be imposed. By mixing an oxygen saturated and oxygen-free stream, DO fluctuations may also be imposed. Laminar flow means there will be axial dispersion, which has to be quantified.

A 2D CFD simulation of a feed pulse in a microfluidic system was done as a proof-of-principle, the geometry being a simplification of a cell-trap design [79], shown in Fig. 10A. A 40 µm diameter was set for the feed- and main flow channels. Both inlets had a liquid inlet velocity of $5–20 \times 10^{-4}$ m/s, making the main channel velocity 1–4 mm/s. The path length was approx. 3 mm/s. First, the flow was solved in steady state with pure fluid *B*. At $t = 0$, inlet 1 is switched to pure *A*, with properties equal to *B* and a molecular diffusion coefficient $\mathcal{D}_m = 6 \times 10^{-10}\,\mathrm{m^2/s}$. Fig. 10A shows a snapshot of the transition from *B* to *A* + *B*. After 3 s, inlet 1 switched back to *B*. The concentration of *A* at the cell cluster was measured. While the imposed step is indeed dispersed somewhat, a change from 5 to 95% saturation takes just 0.46–1.15 s (Fig. 11), for the highest and lowest simulated velocity. Still, if required, backmixing may be further reduced by using droplet-based microfluidics to enhance plug flow (Fig. 10B), albeit at the drawback that cells grow in compartments separate from the main flow, requiring diffusion-controlled substrate transfer [80]. In both cases, with a transfer function describing the device dynamics, it can be checked if convolution of imposed dynamics by device dynamics affects the metabolic response. Deconvolution of the device dynamics may be possible if lifeline dynamics are slower than device dynamics. The above conceptual analysis concludes that inducing rapid fluctuations using microreactors is feasible. The challenge likely lies in quantifying the dynamic metabolic response.

6.1.1. Single-cell analysis: towards experimental lifelines?

Several microfluidic studies have focused on visual measurements,

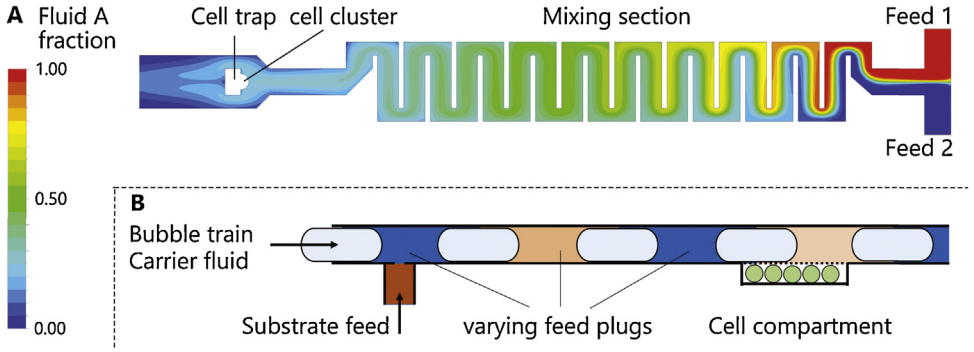

Fig. 10. *A:* 2-D CFD simulation of a simple single-phase micro-reactor (channel diameter 40 µm) designed to impose rapid extra-cellular variations on micro-organisms, physically trapped in a cell chamber. Contour plot shows a switch from pure fluid *B* to fluid *A* fed via feed 1, while feed 2 constantly feeds fluid *B*. *B:* concept layout of a 2-phase microreactor designed to reduce backmixing in the substrate flow by introducing Taylor-flow.

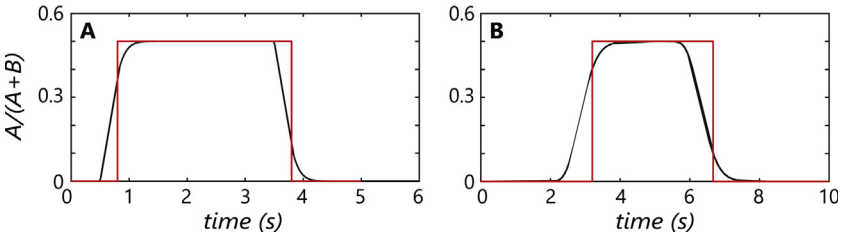

Fig. 11. Response at the cell-trap (black) to a pulse of *A* inserted via one inlet. The pulse profile (red) has been visualized as the response for a perfect plug flow with the same superficial flow-rate. *A:* inlet velocity of 2 mm/s, *B:* inlet velocity of 0.5 mm/s per channel.

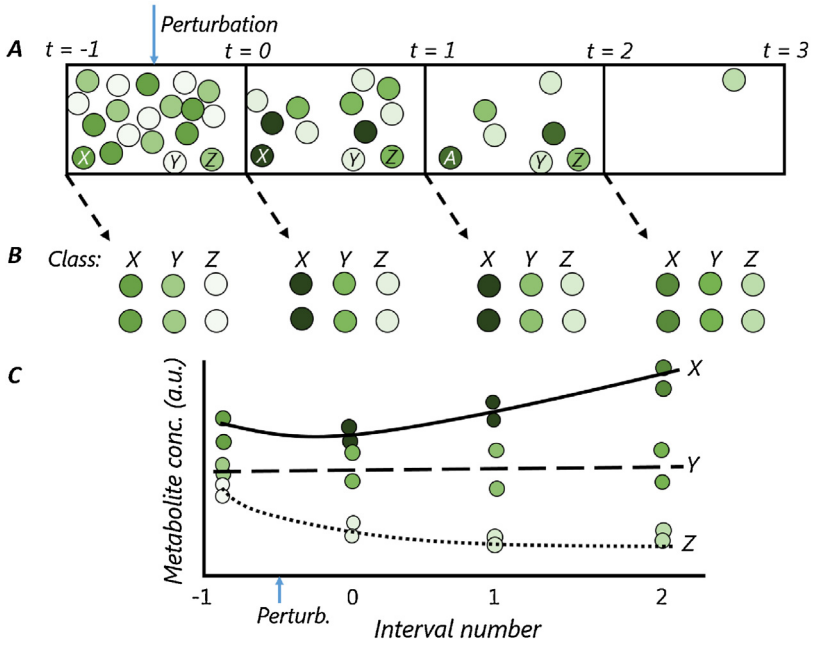

Fig. 12. Conceptual outline of activity segregated lifeline analysis, using three activity classes (called *X*, *Y*, *Z*), defined pre-perturbation. *A:* Microcultivation containing cells with a fast-responding fluorescent label. Samples are taken at regular intervals; an extra-cellular perturbation is introduced between samples −1 and 0. *B:* The samples are sorted and segregated based on their activity class, e.g. using FACS. Due to the fast-responding label, the fluorescence-activity of each class may change in time; this is accounted for by on-line fluorescence monitoring of cells that were grouped in the same activity class. *C:* After sorting, the established sub-populations are analyzed with off-line techniques, for example to measure the abundance of key metabolites (or metabolite classes). The graph illustrates how the dynamic abundance of a key metabolite can be monitored, segregated on fluorescent activity. If the correlation between label activity and composition is strong, this allows to approximate quantitative experimental lifelines. A prerequisite is that samples can be sorted and quenched sufficiently fast to allow metabolite analysis.

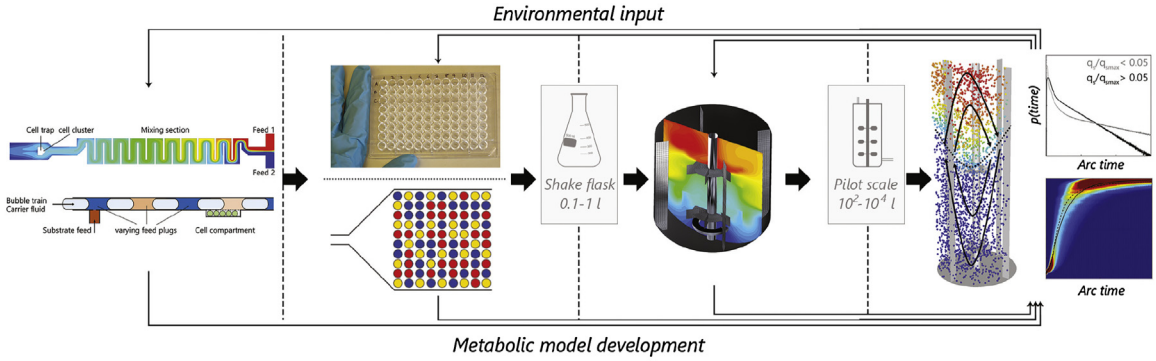

Microfluidics	Parallel well-plate (now)	Lab-scale cultivation	Industrial-scale process
Metabolic understanding:	**Massive Microfluidics (future)**	*Scale down verification*	*(CFD based) environment*
modeling, metabolic triggers	*Strain selection*	*Heterogeneity study*	*quantification*
Single-cell response analysis	*Heterogeneity triggers*	*(population interaction)*	*Production optimization*
Direct lifeline screening	*Operation condition screening*	*Operational verification*	

Fig. 13. Multi-scale bioreactor evaluation and design approach. Micro-fluidics allow single cell or small population analysis. Combined with omics-information from the other lab-scales, this provides a comprehensive modeling basis. The microtiter-scale and/or massive parallel microfluidics provide the environment for rapid parallel strain evaluation and selection, which may make the shake-flask obsolete. The regular bench-scale remains valuable for verification and population behavior. Large-scale (CFD) data feeds environmental information, and is the target for reactor optimization. For well-defined processes, the intermediate pilot scale may in time be omitted.

such as cell division frequency or fluorescent labeling [81,73,76]. These techniques could be employed to study the response of (repetitive) extra-cellular perturbations on the single cell level. Still, many dimensions of the cellular response cannot (currently) be measured on-line, while knowledge about the dynamics of these responses is relevant for modeling purposes, where the overall cellular performance (e.g. growth rate, enzyme expression, production rates) is computed based on the dynamics of a number of intra-cellular pools (metabolites, redox factors, enzymes, etcetera).

Cell-sorting techniques, such as Fluorescence Activated Cell Sorting [82,83] (FACS), offer the option to segregate cells in a (micro)population based. For example, this can be used to segregate a cell-sample in

several classes of cells after a perturbation, based on their fluorescent activity. A range of off-line techniques can then be used for an in-depth analysis of the sub-population characteristics (sub-population omics [84,83]). This allows, for example, to correlate the availability of certain key-metabolites after a perturbation with the strength of the on-line (e.g. fluorescent) response. Such data, providing links between metabolite levels and fluorescent response, is highly useful for modeling purposes. In principle, it is possible quantify certain compound classes or specific metabolites at the single-cell level [85], although their size limits such possibilities for microbes. In cases where the metabolite abundance *is* sufficient, the variance within a given sub-population could be assessed to comment on the intrinsic heterogeneity in such pools, as well as the strength of the correlation to the on-line measured response.

The above methodology can be applied in "classical" bench-scale cultivations, as the activity at time of sorting can be correlated with subsequent measurement data. However, such cultivations do not allow to follow the response of individual cells on-line, meaning that we can only link metabolite levels between timesteps if the fluorescent activity of sub-populations is static: for example, how do metabolite levels after a substrate pulse develop in relation to the abundance of a certain (labeled) enzyme, the level of which does not change in the studied timeframe. If the fluorescent activity itself changes in response to the pulse, for example using fast-responding bio-sensors to monitor the availability of a single key metabolite or signal molecule [86,45,87], it is not possible to reconstruct dynamics: we don't know how the activity of a cell at timestep t relates to that at step $t-1$. In micro-fluidic cultivations establishing such correlations *is* possible, as we can track individual cells in time, thereby allowing to construct dynamic "activity classes". Again, we can take (off-line, destructive) samples of sorted sub-populations and correlate the levels of measured metabolites with the fluorescent response, but now we can also use the on-line single-cell responses to monitor how sub-populations develop in time, in terms of their fluorescent activity and (by correlation) other relevant metabolic pools. If population heterogeneity is already visible prior to a perturbation, it is possible to monitor how different sub-populations respond to a perturbation (how strong is the response, and is it consistent between cells in a class?), in relation to their pre-perturbation composition. Graphically, this approach is outlined in Fig. 12. Of course, we are still typically dealing with sub-population averages, and sub-populations will still be *intrinsically heterogeneous*, hence individual lifelines of cells in the sub-population may still differ. Still, being able to measure and dynamically model *extrinsic* heterogeneity between sub-populations [45] would be a large step forward from the current situation, where models are based on whole-population averages. Significant experimental developments are required to realize experimental lifeline acquisition as described above, but the insights might well be worth pushing for, and we've only just begun to explore the opportunities.

7. Future perspective

Euler–Lagrange CFD simulations, especially with C3 coupling, require days to weeks of computation time to resolve several mixing times of flow time. This limits its applications; routine usage in process design and optimization is not yet feasible. Computational advances such as highly parallelized simulations and GPU-assisted CFD are promising: real-time Euler–Lagrange simulations are already feasible if the flow itself can be considered steady-state, and ANSYS Discovery live already delivers real-time capabilities for transient single-phase flows. If this is extended to multi-phase and reactive flows, application for routine design and optimization are truly within reach. Even if crude meshes are applied, the ability to assess the qualitative impact of design changes and subsequently case the most promising configurations in detail is of great interest. Next-generation microfluidic SD-simulators may then impose lifelines from such simulations directly on organisms, while advances in micro-population omics allow for ever-increasing insight in the cellular response. Our current understanding of extracellular fluctuation effects is insufficient to go directly from lab to full scale, but with increasing understanding the need for piloting may reduce. Automated microwell devices like the Biolector [88] are replacing shake-flasks, allowing for parallelized strain testing, and in due time milli-wells may be replaced by micro-droplet cultivations, converging the capacity of microfluidic micro-population and/or even single-cell analysis with highly parallel strain testing and controlled population heterogeneity studies. The combined information from massive parallel micro-cultivations and bench-scale cultivations refines metabolic understanding and associated CFD-CRD models; these simulations in turn provide environmental input for cultivations at all scales, illustrated in Fig. 13. Real-time simulations also have implications for process control. Imagine a "digital twin" of an industrial reactor, predicting the effect of process disturbances on the metabolic composition; with visualization techniques like virtual reality, operators may even "look" into running processes on-site. While this may be some longer term speculation, the potential is certainly there. Advances in simulation, miniaturization and visualization will impact the field of bioprocess engineering in the years to come, and the biggest advances are likely still ahead.

Acknowledgements

We gratefully acknowledge the input from our colleagues at the DSM biotechnology center, Delft university of Technology, and collaborators at East China University of Technology. We are especially thankful to Wenjun Tang, Guan Wang, Wouter van Winden, Walter van Gulik, Amit Deshmukh, Ju Chu, Jianye Xia, Matthias Reuss and Sef Heijnen for their frequent discussions and contributions to the collaborative project that was the origin of this work. This work has been conducted within a multi-party research project, among DSM-Sinochem Pharmaceuticals, TU Delft, East China University of Science and Technology and Shanghai Guojia Ltd., funded by NWO and MoST (2013DFG32630).

Appendix A. Supplementary data

Supplementary data associated with this article can be found, in the online version, at https://doi.org/10.1016/j.bej.2018.09.001.

References

[1] A. Lapin, D. Müller, M. Reuss, Dynamic behavior of microbial populations in stirred bioreactors simulated with Euler–Lagrange methods: traveling along the lifelines of single cells, Ind. Eng. Chem. Res. 43 (2004) 4647–4656.
[2] A. Lapin, J. Schmid, M. Reuss, Modeling the dynamics of *E. coli* populations in the three-dimensional turbulent field of a stirred-tank bioreactor—a structured-segregated approach, Chem. Eng. Sci. 61 (2006) 4783–4797.
[3] A. Humphrey, Shake flask to fermentor: what have we learned? Biotechnol. Progr. 14 (1998) 3–7.
[4] P. Neubauer, S. Junne, Scale-down simulators for metabolic analysis of large-scale bioprocesses, Curr. Opin. Biotechnol. 21 (2010) 114–121.
[5] G. Wang, W. Tang, J. Xia, J. Chu, H.J. Noorman, W.M. van Gulik, Integration of microbial kinetics and fluid dynamics toward model-driven scale-up of industrial bioprocesses, Eng. Life Sci. 15 (2015) 20–29.
[6] N.M. Oosterhuis, N.W. Kossen, Dissolved oxygen concentration profiles in a production-scale bioreactor, Biotechnol. Bioeng. 26 (1984) 546–550.
[7] A.P.J. Sweere, Y.A. Matla, J. Zandvliet, K.C.A.M. Luyben, N.W.F. Kossen, Experimental simulation of glucose fluctuations, Appl. Microbiol. Biotechnol. 28 (1988) 109–115.
[8] A.P.J. Sweere, J.R. Mesters, L. Janse, K.C.A.M. Luyben, N.W.F. Kossen, Experimental simulation of oxygen profiles and their influence on baker's yeast production: I. One-fermentor system, Biotechnol. Bioeng. 31 (1988) 567–578.
[9] A.P.J. Sweere, L. Janse, K.C.A.M. Luyben, N.W.F. Kossen, Experimental simulation of oxygen profiles and their influence on baker's yeast production: II. Two-fermentor system, Biotechnol. Bioeng. 31 (1988) 579–586.
[10] A. Lemoine, M.H. Limberg, S. Kästner, M. Oldiges, P. Neubauer, S. Junne, Performance loss of Corynebacterium glutamicum cultivations under scale-down conditions using complex media, Eng. Life Sci. (2016).
[11] A.-L. Heins, R. Lencastre Fernandes, K.V. Gernaey, A.E. Lantz, Experimental and in silico investigation of population heterogeneity in continuous Sachharomyces

cerevisiae scale-down fermentation in a two-compartment setup, J. Chem. Technol. Biotechnol. 90 (2015) 324–340.
[12] L.P. de Jonge, N.A.A. Buijs, A. ten Pierick, A. Deshmukh, Z. Zhao, J.A.K.W. Kiel, J.J. Heijnen, W.M. van Gulik, Scale-down of penicillin production in *Penicillium chrysogenum*, Biotechnol. J. 6 (2011) 944–958.
[13] A. Sweere, K. Luyben, N. Kossen, Regime analysis and scale-down: tools to investigate the performance of bioreactors, Enzyme Microb. Technol. 9 (1987) 386–398.
[14] G. Larsson, M. Törnkvist, E.S. Wernersson, C. Trägårdh, H. Noorman, S.O. Enfors, Substrate gradients in bioreactors: origin and consequences, Bioprocess. Eng. 14 (1996) 281–289.
[15] J.J.J. Gillissen, H.E.A. Van den Akker, Direct numerical simulation of the turbulent flow in a baffled tank driven by a Rushton turbine, AIChE J. 58 (2012) 3878–3890.
[16] M. Coroneo, G. Montante, A. Paglianti, F. Magelli, CFD prediction of fluid flow and mixing in stirred tanks: numerical issues about the RANS simulations, Comput. Chem. Eng. 35 (2011) 1959–1968.
[17] H. Hartmann, J.J. Derksen, H.E.A. van den Akker, Mixing times in a turbulent stirred tank by means of LES, AIChE J. 52 (2006) 3696–3706.
[18] J. Gimbun, C. Rielly, Z. Nagy, Modelling of mass transfer in gas–liquid stirred tanks agitated by Rushton turbine and CD-6 impeller: a scale-up study, Chem. Eng. Res. Des. 87 (2009) 437–451.
[19] J.-C. Gabelle, F. Augier, A. Carvalho, R. Rousset, J. Morchain, Effect of tank size on kLa and mixing time in aerated stirred reactors with non-Newtonian fluids, Can. J. Chem. Eng. 89 (2011) 1139–1153.
[20] G. Wang, J. Chu, H.J. Noorman, J. Xia, W. Tang, Y. Zhuang, S. Zhang, Prelude to rational scale-up of penicillin production: a scale-down study, Appl. Microbiol. Biotechnol. 98 (2014) 2359–2369.
[21] O. Gunyol, H.J. Noorman, R.F. Mudde, CFD simulations of a large-scale fermenter with multiple impellers, in: P. Chaouki, J. Tanguy (Eds.), Proceedings of the 9th International Conference on Gas–Liquid Solid Reactor Engineering, Montreal, 2009, pp. 1–4.
[22] C. Haringa, A.T. Deshmukh, R.F. Mudde, H.J. Noorman, Euler–Lagrange analysis towards representative down-scaling of a 22m3 aerobic *S. cerevisiae* fermentation, Chem. Eng. Sci. 170 (2017) 653–669.
[23] M. Linkès, P. Fede, J. Morchain, P. Schmitz, Numerical investigation of subgrid mixing effects on the calculation of biological reaction rates, Chem. Eng. Sci. 116 (2014) 473–485.
[24] J. Douaire, A. Morchain, Liné, Relationship between hydrodynamic conditions and substrate influx towards cells, 13th European Conference on Mixing (2009) 14–17.
[25] M. Linkès, M. Martins Afonso, P. Fede, J. Morchain, P. Schmitz, Numerical study of substrate assimilation by a microorganism exposed to fluctuating concentration, Chem. Eng. Sci. 81 (2012) 8–19.
[26] J.A. Roels, J. Van Den Berg, R.M. Voncken, The rheology of mycelial broths, Biotechnol. Bioeng. 16 (1974) 181–208.
[27] P. Moilanen, M. Laakkonen, O. Visuri, J. Aittamaa, Modeling local gas–liquid mass transfer in agitated viscous shear-thinning dispersions with CFD, Ind. Eng. Chem. Res. 46 (2007) 7289–7299.
[28] A. Dehbi, A CFD model for particle dispersion in turbulent boundary layer flows, Nucl. Eng. Des. 238 (2008) 707–715.
[29] C. Haringa, H.J.H.H.J. Noorman, R.F.R. Mudde, Lagrangian modeling of hydrodynamic–kinetic interactions in (bio)chemical reactors: practical implementation and setup guidelines, Chem. Eng. Sci. 157 (2017) 159–168.
[30] O. Gunyol, R.F. Mudde, Computational study of hydrodynamics of a standard stirred tank reactor and a large-scale multi-impeller fermenter, Int. J. Multiscale Comput. Eng. 7 (2009) 559–576.
[31] M. Pigou, J. Morchain, Investigating the interactions between physical and biological heterogeneities in bioreactors using compartment, population balance and metabolic models, Chem. Eng. Sci. 126 (2014) 267–282.
[32] D.D. McClure, J.M. Kavanagh, D.F. Fletcher, G.W. Barton, Characterizing bubble column bioreactor performance using computational fluid dynamics, Chem. Eng. Sci. 144 (2016) 58–74.
[33] C. Haringa, W. Tang, G. Wang, A.T.A. Deshmukh, W.A.W. van Winden, J. Chu, W.W.M. van Gulik, J.J.J. Heijnen, R.R.F. Mudde, H.J.H. Noorman, Computational fluid dynamics simulation of an industrial P. chrysogenum fermentation with a coupled 9-pool metabolic model: towards rational scale-down and design optimization, Chem. Eng. Sci. 175 (2018) 12–24.
[34] M. Löffler, J.D. Simen, G. Jäger, K. Schäferhoff, A. Freund, R. Takors, Engineering *E. coli* for large-scale production – strategies considering ATP expenses and transcriptional responses, Metab. Eng. 38 (2016) 73–85.
[35] J.D. Simen, M. Löffler, G. Jäger, K. Schäferhoff, A. Freund, J. Matthes, J. Müller, R. Takors, Transcriptional response of Escherichia coli to ammonia and glucose fluctuations, Microb. Biotechnol. 10 (2017) 858–872.
[36] A. Nieß, M. Löffler, J.D. Simen, R. Takors, Repetitive short-term stimuli imposed in poor mixing zones induce long-term adaptation of *E. coli* cultures in large-scale bioreactors: experimental evidence and mathematical model, Front. Microbiol. 8 (2017) 1195.
[37] A. Nieß, J. Failmezger, M. Kuschel, M. Siemann-Herzberg, R. Takors, Experimentally validated model enables debottlenecking of in vitro protein synthesis and identifies a control shift under in vivo conditions, ACS Synth. Biol. 6 (2017) 1913–1921.
[38] M. Kuschel, F. Siebler, R. Takors, Lagrangian trajectories to predict the formation of population heterogeneity in large-scale bioreactors, Bioengineering 4 (2017) 27.
[39] C. Haringa, W. Tang, A.A.T. Deshmukh, J. Xia, M. Reuss, J.J. Heijnen, R.F.R. Mudde, H.H.J. Noorman, Euler–Lagrange computational fluid dynamics for (bio)reactor scale down: an analysis of organism lifelines, Eng. Life Sci. 16 (2016) 652–663.
[40] J. Morchain, J.-C. Gabelle, A. Cockx, Coupling of biokinetic and population balance models to account for biological heterogeneity in bioreactors, AIChE J. 59 (2013) 369–379.
[41] J. Morchain, J.-C. Gabelle, A. Cockx, A coupled population balance model and CFD approach for the simulation of mixing issues in lab-scale and industrial bioreactors, AIChE J. 60 (2014) 27–40.
[42] M. Pigou, J. Morchain, P. Fede, M.-I. Penet, G. Laronze, An assessment of methods of moments for the simulation of population dynamics in large-scale bioreactors, Chem. Eng. Sci. 171 (2017) 218–232.
[43] M. Pigou, J. Morchain, P. Fede, M.-I. Penet, G. Laronze, New developments of the extended quadrature method of moments to solve population balance equations, J. Comput. Phys. 365 (2018) 243–268.
[44] V. Quedeville, H. Ouazaite, B. Polizzi, R. Fox, P. Villedieu, P. Fede, F. Létisse, J. Morchain, A two-dimensional population balance model for cell growth including multiple uptake systems, Chem. Eng. Res. Des. 132 (2018) 966–981.
[45] F. Delvigne, H. Pêcheux, C. Tarayre, Fluorescent reporter libraries as useful tools for optimizing microbial cell factories: a review of the current methods and applications, Front. Bioeng. Biotechnol. 3 (2015) 147.
[46] P. Labhsetwar, J.A. Cole, E. Roberts, N.D. Price, Z.A. Luthey-Schulten, Heterogeneity in protein expression induces metabolic variability in a modeled Escherichia coli population, Proc. Natl. Acad. Sci. U. S. A. 110 (2013) 14006–14011.
[47] W. Tang, A.A.T. Deshmukh, C. Haringa, G. Wang, W. van Gulik, W. van Winden, M. Reuss, J.J. Heijnen, J. Xia, J. Chu, H.H.J. Noorman, A 9-pool metabolic structured kinetic model describing days to seconds dynamics of growth and product formation by *Penicillium chrysogenum*, Biotechnol. Bioeng. 114 (2017) 1733–1743.
[48] F. Lei, M. Rotbøll, S.B. Jørgensen, A biochemically structured model for *Saccharomyces cerevisiae*, J. Biotechnol. 88 (2001) 205–221.
[49] D. Guha, M.P. Dudukovic, P.A. Ramachandran, S. Mehta, J. Alvare, CFD-based compartmental modeling of single phase stirred-tank reactors, AIChE J. 52 (2006) 1836–1846.
[50] A. Delafosse, M.-L. Collignon, S. Calvo, F. Delvigne, M. Crine, P. Thonart, D. Toye, CFD-based compartment model for description of mixing in bioreactors, Chem. Eng. Sci. 106 (2014) 76–85.
[51] F. Delvigne, J. Destain, P. Thonart, Structured mixing model for stirred bioreactors: an extension to the stochastic approach, Chem. Eng. J. 113 (2005) 1–12.
[52] F. Delvigne, J. Destain, P. Thonart, A methodology for the design of scale-down bioreactors by the use of mixing and circulation stochastic models, Biochem. Eng. J. 28 (2006) 256–268.
[53] F. Delvigne, A. Lejeune, J. Destain, P. Thonart, Stochastic models to study the impact of mixing on a fed-batch culture of *Saccharomyces cerevisiae*, Biotechnol. Progr. 22 (2006) 259–269.
[54] A. Delafosse, S. Calvo, M.-L. Collignon, F. Delvigne, M. Crine, D. Toye, Euler–Lagrange approach to model heterogeneities in stirred tank bioreactors – comparison to experimental flow characterization and particle tracking, Chem. Eng. Sci. 134 (2015) 457–466.
[55] G. Wang, J. Zhao, C. Haringa, W. Tang, J. Xia, J. Chu, Y. Zhuang, S. Zhang, A.T.A. Deshmukh, W. van Gulik, J.J.J. Heijnen, H.J.H. Noorman, Comparative performance of different scale-down simulators of substrate gradients in *Penicillium chrysogenum* cultures: the need of a biological systems response analysis, Microb. Biotechnol. 11 (2018).
[56] S.-O. Enfors, M. Jahic, A. Rozkov, B. Xu, M. Hecker, B. Jürgen, E. Krüger, T. Schweder, G. Hamer, D. O'Beirne, N. Noisommit-Rizzi, M. Reuss, L. Boone, C. Hewitt, C. McFarlane, A. Nienow, T. Kovacs, C. Trägårdh, L. Fuchs, J. Revstedt, P. Friberg, B. Hjertager, G. Blomsten, H. Skogman, S. Hjort, F. Hoeks, H.-Y. Lin, P. Neubauer, R. van der Lans, K. Luyben, P. Vrabel, Å. Manelius, Physiological responses to mixing in large scale bioreactors, J. Biotechnol. 85 (2001) 175–185.
[57] R. Rosello Sastre, Z. Csögör, I. Perner-Nochta, P. Fleck-Schneider, C. Posten, Scale-down of microalgae cultivations in tubular photo-bioreactors – a conceptual approach, J. Biotechnol. 132 (2007) 127–133.
[58] R. Legmann, H.B. Schreyer, R.G. Combs, E.L. Mccormick, A.P. Russo, S.T. Rodgers, A predictive high-throughput scale-down model of monoclonal antibody production in CHO cells, Biotechnol. Bioeng. 104 (2009) 1107–1120.
[59] P. Vrábel, R. Van der Lans, Y. Cui, K. Luyben, Compartment model approach, Chem. Eng. Res. Des. 77 (1999) 291–302.
[60] P. Vrábel, R.G. van der Lans, K.C. Luyben, L. Boon, A.W. Nienow, Mixing in large-scale vessels stirred with multiple radial or radial and axial up-pumping impellers: modelling and measurements, Chem. Eng. Sci. 55 (2000) 5881–5896.
[61] P. Vrábel, R.G. van der Lans, F.N. van der Schot, K.C. Luyben, B. Xu, S.-O. Enfors, CMA: integration of fluid dynamics and microbial kinetics in modelling of large-scale fermentations, Chem. Eng. J. 84 (2001) 463–474.
[62] A. Lemoine, N. Maya Martinez-Iturralde, R. Spann, P. Neubauer, S. Junne, Response of *Corynebacterium glutamicum* exposed to oscillating cultivation conditions in a two- and a novel three-compartment scale-down bioreactor, Biotechnol. Bioeng. 112 (2015) 1220–1231.
[63] E. Postma, C. Verduyn, W.A. Scheffers, J.P. Van Dijken, Enzymic analysis of the crabtree effect in glucose-limited chemostat cultures of *Saccharomyces cerevisiae*, Appl. Environ. Microbiol. 55 (1989) 468–477.
[64] H. Noorman, An industrial perspective on bioreactor scale-down: what we can learn from combined large-scale bioprocess and model fluid studies, Biotechnol. J. 6 (2011) 934–943.
[65] M. Šimčík, A. Mota, M. Ruzicka, A. Vicente, J. Teixeira, CFD simulation and experimental measurement of gas holdup and liquid interstitial velocity in internal loop airlift reactor, Chem. Eng. Sci. 66 (2011) 3268–3279.
[66] M. Gavrilescu, R.Z. Tudose, Residence time distribution of the liquid phase in a concentric-tube airlift reactor, Chem. Eng. Process. 38 (1999) 225–2238.

[67] A. Essadki, B. Gourich, C. Vial, H. Delmas, Residence time distribution measurements in an external-loop airlift reactor: study of the hydrodynamics of the liquid circulation induced by the hydrogen bubbles, Chem. Eng. Sci. 66 (2011) 3125–3132.
[68] O. Simonin, P. Viollet, Modeling of turbulent two-phase jets loaded with discrete particles, Phenom. Multiph. Flows (1990) 259–269.
[69] C. Haringa, Through the Organism's Eyes: The Interaction between Hydrodynamics and Metabolic Dynamics in Industrial-Scale Fermentation Processes (Ph.D. thesis), Delft University of Technology, 2017.
[70] Y. Liu, Z.-J. Wang, J.-y. Xia, C. Haringa, Y.-p. Liu, J. Chu, Y.-P. Zhuang, S.-L. Zhang, Application of Euler–Lagrange CFD for quantitative evaluating the effect of shear force on *Carthamus tinctorius* L. cell in a stirred tank bioreactor, Biochem. Eng. J. 114 (2016) 209–217.
[71] P. Jüsten, G.C. Paul, A.W. Nienow, C.R. Thomas, Dependence of *Penicillium chrysogenum* growth, morphology, vacuolation, and productivity in fed-batch fermentations on impeller type and agitation intensity, Biotechnol. Bioeng. 59 (1998) 762–775.
[72] S. Kim, H.J. Kim, N.L. Jeon, Biological applications of microfluidic gradient devices, Integr. Biol. 2 (2010) 584.
[73] A. Grünberger, W. Wiechert, D. Kohlheyer, Single-cell microfluidics: opportunity for bioprocess development, Curr. Opin. Biotechnol. 29 (2014) 15–23.
[74] A. Grünberger, C. Probst, S. Helfrich, A. Nanda, B. Stute, W. Wiechert, E. von Lieres, K. Nöh, J. Frunzke, D. Kohlheyer, Spatiotemporal microbial single-cell analysis using a high-throughput microfluidics cultivation platform, Cytometry Part A 87 (2015) 1101–1115.
[75] A.F. Oliveira, A.C.S.N. Pessoa, R.G. Bastos, L.G. de la Torre, Microfluidic tools toward industrial biotechnology, Biotechnol. Progr. 32 (2016) 1372–1389.
[76] A. Grünberger, K. Schöler, C. Probst, G. Kornfeld, T. Hardiman, W. Wiechert, D. Kohlheyer, S. Noack, Real-time monitoring of fungal growth and morphogenesis at single-cell resolution, Eng. Life Sci. 17 (2017) 86–92.
[77] G. Lambert, E. Kussell, J. Heuveling, V. Wendisch, R. Hengge, Memory and fitness optimization of bacteria under fluctuating environments, PLoS Genet. 10 (2014) e1004556.
[78] M.R. Bennett, J. Hasty, Microfluidic devices for measuring gene network dynamics in single cells, Nat. Rev. Genet. 10 (2009) 628–638.
[79] C. Probst, A. Grünberger, W. Wiechert, D. Kohlheyer, Polydimethylsiloxane (PDMS) sub-micron traps for single-cell analysis of bacteria, Micromachines 4 (2013) 357–369.
[80] C. Westerwalbesloh, A. Grünberger, B. Stute, S. Weber, W. Wiechert, D. Kohlheyer, E. von Lieres, Modeling and CFD simulation of nutrient distribution in picoliter bioreactors for bacterial growth studies on single-cell level, Lab Chip 15 (2015) 4177–4186.
[81] A. Grünberger, N. Paczia, C. Probst, G. Schendzielorz, L. Eggeling, S. Noack, W. Wiechert, D. Kohlheyer, A disposable picolitre bioreactor for cultivation and investigation of industrially relevant bacteria on the single cell level, Lab Chip 12 (2012) 2060.
[82] L.A. Herzenberg, D. Parks, B. Sahaf, O. Perez, M. Roederer, L.A. Herzenberg, The history and future of the fluorescence activated cell sorter and flow cytometry: a view from stanford, Clin. Chem. 48 (2002) 1819–1827.
[83] M. Jahn, C. Vorpahl, D. Tü, M. Lindmeyer, B. Bü, H. Harms, S. Mü, Accurate determination of plasmid copy number of flow-sorted cells using droplet digital PCR, Anal. Chem. 86 (2014) 5969–5976.
[84] M. Jahn, J. Seifert, M. von Bergen, A. Schmid, B. Bühler, Subpopulation-proteomics in prokaryotic populations, Curr. Opin. Biotechnol. 24 (2013) 79–87.
[85] A.E. Vasdekis, G. Stephanopoulos, Review of methods to probe single cell metabolism and bioenergetics, Metab. Eng. 27 (2015) 115–135.
[86] F. Delvigne, P. Goffin, Microbial heterogeneity affects bioprocess robustness: dynamic single-cell analysis contributes to understanding of microbial populations, Biotechnol. J. 9 (2014) 61–72.
[87] A. Lemoine, F. Delvigne, A. Bockisch, P. Neubauer, S. Junne, Tools for the determination of population heterogeneity caused by inhomogeneous cultivation conditions, J. Biotechnol. 251 (2017) 84–93.
[88] M. Funke, A. Buchenauer, U. Schnakenberg, W. Mokwa, S. Diederichs, A. Mertens, C. Müller, F. Kensy, J. Büchs, Microfluidic biolector-microfluidic bioprocess control in microtiter plates, Biotechnol. Bioeng. 107 (2010) 497–505.